



A study of the step-flow growth of the PVT-grown AlN crystals by multi-scale modeling method

Journal:	<i>CrystEngComm</i>
Manuscript ID:	CE-ART-01-2014-000175.R1
Article Type:	Paper
Date Submitted by the Author:	27-Mar-2014
Complete List of Authors:	Guo, Wei; University of Bayreuth, Material and Process Simulation (MPS) Kundin, Julia; Univeristy of Bayreuth, Material and Process Simulation (MPS) Bickermann, Matthias; Leibniz-Institut fur Kristallzuchtung (IKZ), Emmerich, Heike; Univeristy of Bayreuth, Material and Process Simulation (MPS)

Title: A study of the step-flow growth of the PVT-grown AlN crystals by multi-scale modeling method

Authors:

Wei Guo^a, Julia Kundin^a, Matthias Bickermann^b, Heike Emmerich^a

^a Department of Materials and Process Simulations, University Bayreuth, Bayreuth, Germany

^b Leibniz-Institute for crystallization (IKZ), Berlin, Germany

*Corresponding author:

Tel: +49 (0)921/55-7882

E-mail: wei.guo@uni-bayreuth.de

Postal address:

Material and Process Simulations (MPS)

University Bayreuth

Postfach 10 12 51

D-95440 Bayreuth, Germany

Abstract:

A kinetic Monte Carlo (KMC) model coupled with the vapor diffusion above the Al-polar (0001) surface of AlN is constructed for the physical vapor transport (PVT) growth of AlN crystal. Most of the important surface events and the vapor diffusion of Al atoms are taken into account. Based on the numerical simulations, an analytical model of the step-flow growth on (0001) surface is attained and the time evolution of random terrace widths under homogeneous and linearly inhomogeneous vapor flux of Al atoms is explored. By the KMC model and the analytical model it is found that under the growing conditions of this work the rate limiting step for the PVT growth of AlN is the supply of Al atoms due to the tiny flow of Al atoms in the vapor phase (Al_g) at the steady state. The energy barriers for adsorbed AlN (AlN_{ad}) incorporating at different configurations of neighboring AlN dimers can influence the growth morphology significantly. If the adsorption rate of Al_g is much slower than the rates of the surface events, the step-bunching caused by the randomness of the terrace widths can be avoided under either the homogeneous or linearly inhomogeneous flux of Al_g .

Key words:

A1. growth models; A1. computer simulation; A3. physical vapor deposition processes; B1. nitrides; A2. surface structure; A1. morphology stability

1. Introduction

AlN as a semiconductor is very promising for realizing high efficiency deep ultraviolet light-emitting diodes (UV-LEDs) which is of considerable interest for applications such as sterilization, water purification, medicine and biochemistry, light sources for high density optical recording, etc. [1–3]. AlN layers have been grown on foreign substrates like sapphire and silicon carbide. The density of threading dislocations in AlN layers is high because of the lattice-mismatch between the AlN layer and the foreign substrate and this is a major obstacle to improving light emitting efficiency [4, 5]. Recently, AlN bulk single crystals have been developed as substrates for the growth of AlN layers, and due to the match between the layer and the substrate the UV devices grown on the native substrate have a significant improvement in their performance [6, 7]. Currently, the physical vapor transport (PVT) growth method is the only approach to produce bulk AlN crystals of high quality and appropriate size for use as substrates and in an acceptable growth speed. The AlN single crystal growth by PVT method is illustrated in Fig. 1. A source of sintered AlN is sublimed at the temperature T_s . The crucible gas consists of the vapor phase from the sublimation of AlN source and the ambient N_2 gas. The temperature of the AlN single crystal seed, T_c , is lower than T_s . Hence the vapor phase from sublimation condenses on the seed and the seed can thus grow into a larger single crystal. The crystal surface vertical to the axis of the crucible is the (0001) surface. The growth of the AlN crystal is mainly due to the motion of the (0001) surface.

The growth of AlN is greatly influenced by the growing conditions. There are several possible

reactions occurring on the (0001) surface of an AlN crystal and they are coupling with each other. It is unclear which ones are the main rate limiting steps. Hence one of the aims of the present work is to explore the relations among different reactions and events on the (0001) surface to gain more insights on the rate limiting steps. Besides the growth rate, the crystal quality is also a main issue in AlN growth. The crystal quality is closely related to the growth modes of the crystal surfaces. Very often, the surfaces of the AlN crystal grow in the step-flow mode and the spiral-dislocation mode. The latter can be considered as a special type of step-flow growth as well. The stable step-flow growth produces faceted surfaces with only few defects. On the contrary, instabilities of the step-flow growth such as step-bunching will produce more defects. The other aim of this work is to investigate the stability of step-flow growth of AlN by means of numerical methods.

The rest of the paper is organized as follows. First, a kinetic Monte Carlo (KMC) model taking into account the reactions on the surface of AlN is developed and it is coupled to the diffusion model of Al atoms in the vapor phase, Al_g . Then the growth of (0001) surface of AlN is studied. After that an analytical model of the step motions is proposed based on the results of the vapor diffusion coupled KMC model. Last the influence of homogeneous and linearly inhomogeneous vapor fluxes of Al atoms on the stability of step-flow growth with random initial terrace widths is studied by the analytical model.

2. KMC simulation of the growth of the Al-polar (0001) surface of AlN

2.1. KMC model

The KMC method [8, 9] describes the time evolution of a system by the stochastic processes.

For a configuration of a system, the total rate, R_{tot} , of all the possible stochastic processes is calculated using the equation:

$$R_{\text{tot}} = \sum_i R_i \quad (1)$$

where R_i is the rate of the process i . Then two uniform random numbers ρ_1 and ρ_2 which are between 0 and 1 are chosen. One integer number p is determined by

$$\sum_{i=0}^{p-1} R_i < \rho_1 R_{\text{tot}} \leq \sum_{i=0}^p R_i \quad (2)$$

Then process p is performed. The simulation time is evaluated as [10]

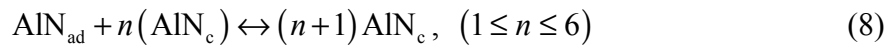
$$t_c \rightarrow t_p - \ln(\rho_2) / R_{\text{tot}} \quad (3)$$

where t_c is the current time and t_p is the previous time.

In the current KMC model a composed hexagonal lattice which consists of three rhomboidal lattices is used to simulate the lattice structure of (0001) of AlN. The size of each rhomboidal lattice is $n_x \times n_y$. The atomic positions are mapped to the composed lattice. The types of the particles included in the KMC model are the Al atoms adsorbed on the surface of the crystal (Al_{ad}), the nitrogen atoms adsorbed on the surface (N_{ad}), the AlN molecules adsorbed on the surface (AlN_{ad}) and the AlN dimer of the single crystal (AlN_{c}). The substrate of the above units is constructed by AlN_{c} . The reactions, the growth processes and the rates of the KMC model are introduced in what follows.

2.1.1. Reactions and growth processes

It is assumed that the PVT growth of an AlN crystal includes the following reactions:



The whole process of AlN crystal growth is modeled as follows. First, Al_g are adsorbed to the (0001) surface of the AlN single crystal seed (Reaction (4)). Then one N_2 molecule reacts with one Al_{ad} atom, producing one AlN_{ad} molecule and one N_{ad} atom (Reaction (5)). Next, the N_{ad} atom reacts with another Al_{ad} atom on the surface and an AlN_{ad} molecule is formed (Reaction (6)). Meanwhile two N_{ad} atoms can meet, react into N_2 gas and leave the surface [11]. At last, the AlN_{ad} molecules grow to the crystal as AlN_c (Reaction (8)). n in Reaction (8) is the number of neighboring AlN_c dimers. The meaning of n will be explained in details in Subsection 2.1.2..

In the above growth model, reaction (5) and (6) replace the usually used reaction $\text{N}_2(g) = \text{N}_{2ads} = 2\text{N}_{ads}$ [12, 13], which means it is assumed in the current model that the direct adsorption of a N_2 molecule to the AlN surface has a negligible success rate. Reaction (5) is

possible because Al has a catalytic effect on the decomposition of N_2 molecules [14]. Reaction (5) and (6) explain how a N_2 molecule can react with an Al_{ad} atom despite the fact that the N–N bond is very strong and the possibility that two Al_{ad} atoms locate at the right positions simultaneously is very low.

2.1.2. The events included in the KMC model

The events in the KMC model are listed in Table 1 (The rates of the events therein will be used shortly.). The surface diffusion of N_{ad} consists of 3 different cases, which are surface diffusion within one terrace, surface diffusion downwards to the next lower terrace and surface diffusion upwards to the next higher terrace. These three surface diffusions are considered as different events in the model. Although the event of the nucleation of a new layer can be integrated into the model easily, the present work focus on the motion of the steps so the nucleation event is not included.

For the reaction (8), the AlN_{ad} produced by reaction (5) and (6) might be transformed into AlN_c depending on the number of neighboring AlN_c dimers. This actually means an incorporation of AlN_{ad} into the crystal because AlN_c is immobile and does not react. For a fixed number of neighbors their positions could be different – all possible configurations are listed in Table 2. In this work it is assumed that for a given number of neighbors there is no influence of configuration on the rate of turning AlN_{ad} into AlN_c . The case of $n = 0$ is considered as a special case of the nucleation of a new layer. Since the nucleation of a new layer is not considered in this work the case of $n = 0$ is not included in Table 2. During the

growth of the crystal, all the growth configurations in Table 2 will be met. For reaction (6) the newly formed AlN_{ad} sits on the position of Al_{ad} after the reaction because it is assumed that AlN_{ad} and Al_{ad} have the same available positions [15].

2.1.3. The rates of the events

The rates for the surface diffusion of Al_{ad} , N_{ad} and AlN_{ad} and reactions (5) and (8) are calculated by

$$R_i = \Gamma_0 \exp(-E_i / k_B T) \quad (9)$$

where R_i is the rate for the event i ; Γ_0 is the attempt frequency of Al_{ad} , N_{ad} or AlN_{ad} ; E_i is the energy barrier for the event i ; k_B is Boltzmann constant; T is temperature. R_i defined here as well as R_{r6} , R_{r7} , and R_{r4} defined in the following are the counter-parts of R_i in Eq. (1). The rate of reaction (6), R_{r6} , is expressed as

$$R_{r6} = \left(\Gamma_0 \exp(-E_{Al}^{diff} / k_B T) + \Gamma_0 \exp(-E_N^{diff} / k_B T) \right) \cdot \exp(-E_{r6} / k_B T) \quad (10)$$

where E_{Al}^{diff} is the energy barrier for the surface diffusion of Al_{ad} ; E_N^{diff} is the energy barrier for the surface diffusion of N_{ad} ; the term $\left(\Gamma_0 \exp(-E_{Al}^{diff} / k_B T) + \Gamma_0 \exp(-E_N^{diff} / k_B T) \right)$ is the knocking rate between Al_{ad} and N_{ad} . E_{r6} is the energy barrier for the reaction (6). Similarly, the rate of reaction (7) is expressed as

$$R_{r7} = 2\Gamma_0 \exp(-E_N^{diff} / k_B T) \cdot \exp(-E_{r7} / k_B T) \quad (11)$$

where $2\Gamma_0 \exp(-E_N^{diff} / k_B T)$ is the knocking rate between two neighboring N_{ad} ; E_{r4} is the

energy barrier for the reaction (7). The rate of reaction (4), R_{r4} , is calculated by

$$R_{r4} = J_{Al}^{in} \cdot S_{Al}^{ad} \quad (12)$$

where J_{Al}^{in} is the flux of Al_g approaching the surface of the single crystal. S_{Al}^{ad} is the area of one available position for the Al_{ad} , which is shown in Fig. 2. J_{Al}^{in} is obtained by Hertz-Knudsen equation:

$$J_{Al}^{in} = \alpha_{Al} \frac{P_{Al}^c}{\sqrt{2\pi m_{Al} k_B T_c}} \quad (13)$$

where α_{Al} is the condensation coefficient of Al_g to the AlN crystal, which is equal to $\Gamma_{success} / \Gamma_{total}$, where Γ_{total} is the total knocking rate of Al_g to the crystal surface of $1m^2$; $\Gamma_{success}$ is the successful knocking rate by which one Al_g is adsorbed by the surface. m_{Al} is the mass of Al atom. T_c is the temperature at the growth interface (assumed to be constant during growth). P_{Al}^c is the pressure of Al vapor next to the surface of AlN crystal and it is derived as

$$P_{Al}^c = c_{Al}^c RT_c \quad (14)$$

where c_{Al}^c is the molar volume concentration of Al_g next to the surface of the AlN crystal; R is the gas constant.

2.2. Vapor diffusion model and its coupling to the KMC model

Since the ambient vapor pressure to be studied in this work is low, the convection effect in the vapor phase is neglected. The transport of Al atoms from the source material to the single

crystal through the vapor phase is modeled as a 1D diffusion process. The vapor diffusion equation follows Fick's second law:

$$\frac{dc}{dt} = -D_v \frac{d^2c}{dx^2}. \quad (15)$$

where c is the molar volume concentration of Al_g ; D_v is the vapor diffusion coefficient of Al_g atoms.

The more critical part of the vapor diffusion model are the two boundary conditions (BCs) of Eq. (15). The physical meanings of the BCs are the flux of Al atoms coming from the source into the vapor phase (BC1) and the flux going from the vapor phase into the single crystal adlayer (BC2). The flux of Al atoms coming out of the source (BC1) is modeled by the Hertz-Knudsen equation:

$$J_{\text{Al}}^{\text{out}} = \alpha_{\text{Al}} \frac{P_{\text{Al}}^e - P_{\text{Al}}^s}{\sqrt{2\pi m_{\text{Al}} k_B T_s}} \quad (16)$$

where $J_{\text{Al}}^{\text{out}}$ is the flux of Al atoms coming out of the AlN source; P_{Al}^s is the pressure of Al vapor next to the surface of AlN source; P_{Al}^e is the pressure of Al_g equilibrium with AlN source at temperature T_s . P_{Al}^e at temperature T_s is derived from the equations:

$$P_{\text{Al}}^e + P_{\text{N}_2}^e = P_{\text{tot}} \quad (17)$$

$$\left(P_{\text{Al}}^e\right)^{-1} \cdot \left(P_{\text{N}_2}^e\right)^{-0.5} = K(T_s) \quad (18)$$

where $P_{\text{N}_2}^e$ is the pressure of N_2 in equilibrium with AlN source at temperature T_s ; P_{tot} is

the total vapor pressure of the system; $K(T)$ is the equilibrium constant at temperature T for the reaction:



Equation (17) is applied because the rate of sublimation is very low and therefore these processes are very close to the equilibrium state. It is also because the vast major species in the vapor phase are Al_g and N_2 .

The flux of Al atoms going from the vapor phase into the single crystal adlayer (BC2) is determined in the following way. First, the KMC model is run for a period of time, Δt_{KMC} , which is expressed as:

$$\Delta t_{\text{KMC}} = \sum_{i=1}^{n_{\text{KMC}}} \Delta t_{\text{KMC}}^i \quad (20)$$

where n_{KMC} is the number of the KMC steps performed during Δt_{KMC} ; Δt_{KMC}^i is the time increase for the i th KMC step. When Δt_{KMC} is equal to the time step Δt_{diff} used in solving the vapor diffusion (Eq. (15)) numerically the amount of Al_g adsorbed to the single crystal obtained by the KMC method during Δt_{KMC} is used as the amount of the Al atoms leaving the vapor phase during Δt_{diff} . On the other hand, since the rate of reaction (4), R_{r4} , is dependent on P_{Al}^c (see Eq. (13)) the KMC simulation is influenced by the vapor diffusion. Thus BC2 serves as the coupling between the vapor diffusion model and the KMC model by transferring the information derived by the KMC model (the amount of Al_g adsorbed to crystal) to the vapor diffusion model (the amount of Al_g leaving the vapor phase) and

performing the influence of the vapor diffusion model (P_{Al}^c) to the KMC model (R_{r4}). As it may be noticed that Δt_{KMC} can not be exactly equal to Δt_{diff} because of the randomness of Δt_{KMC} . Because Δt_{KMC}^i is very small compared with Δt_{diff} the difference between the Δt_{KMC} and Δt_{diff} is very small. Therefore Δt_{KMC} is used as Δt_{diff} in solving the Eq. (15).

2.3. Parameters for the simulation of the growth of (0001) plane by the vapor diffusion coupled KMC model

The input parameters for the simulations are as follows. T_s is 2398 K (2125 °C). T_c is 2348 K (2075 °C). P_{tot} is 0.8 bar. The distance between the source material and the single crystal seed, L_{sc} , is 16 mm. D_v is $6.25 \times 10^{-5} \text{ m}^2 \text{ s}^{-1}$ [16]. α_{Al} is 5×10^{-3} [17], which is the same value as the condensation coefficient of N_2 . m_{Al} is $4.5 \times 10^{-26} \text{ kg}$. $K(T_s)$ in Eq. (18) was obtained by the thermodynamic calculation using the data from JANAF tables [18] and its value is 91.95. P_{Al}^c is $1.22 \times 10^3 \text{ Pa}$ which is derived by solving Eq. (17) and (18). The length of the sides of the regular triangle ABC shown in Fig. 2 is 0.31 nm [19]. Therefore S_{Al}^{ad} is $4.15 \times 10^{-20} \text{ m}^2$. The value used for the attempt frequency of the atoms and the molecules on the surface, Γ_0 , is 10^{12} s^{-1} [20]. The energy barrier for the surface diffusion of Al_{ad} , E_{Al}^{diff} , is 2.2 eV [15]. The energy barrier for the detachment of Al_{ad} , E_{Al}^{det} , is 6.0 eV [15].

The value used for the energy barrier of the surface diffusion of AlN_{ad} , E_{AlN}^{diff} , is 1.78 eV and it is estimated as follows. According to the potential energy surfaces (PESs) of Al_{ad} and N_{ad} [15], the geometrical patterns of the both PESs are the same. The difference is only that the place where the PES of Al_{ad} is maximum, the PES of N_{ad} is minimum and vice versa (see Fig. 3a

and 3b in [15]). It is assumed that the forces acting on the AlN_{ad} is the combination of the forces acting on the Al_{ad} and N_{ad} . Figure 3 shows the overlapping of the PESs of Al_{ad} and N_{ad} on N-terminated (0001) surface of AlN. It is shown that there are two types of positions available for AlN_{ad} . One type is marked by A in Fig. 3. The other type is marked by B. Type A positions have lower energy than type B positions. This agrees with the fact that type A positions are the positions for AlN_{ad} to grow on (0001) surface to form the Wurtzite structure. The energy barriers for B to A and A to B diffusions are 1.64 eV and 2.60 eV respectively. The B to A diffusion and A to B diffusion are reduced to one diffusion event in the KMC simulation by using an average diffusion energy barrier, $E_{\text{AlN}}^{\text{diff}}$, which is defined by

$$\exp\left(-E_{\text{AlN}}^{\text{diff}}/k_{\text{B}}T\right) = \left(\exp\left(-E_{\text{AlN}}^{\text{AB}}/k_{\text{B}}T\right) + \exp\left(-E_{\text{AlN}}^{\text{BA}}/k_{\text{B}}T\right)\right)/2 \quad (21)$$

Equation (21) implies that the diffusion distance of AlN_{ad} obtained using one diffusion event whose barrier is $E_{\text{AlN}}^{\text{diff}}$ is the same as the one obtained using two diffusion events whose barriers are $E_{\text{AlN}}^{\text{AB}}$ and $E_{\text{AlN}}^{\text{BA}}$. By solving Eq. (21) the value of $E_{\text{AlN}}^{\text{diff}}$ is determined as 1.78 eV.

The energy barrier for the diffusion of N_{ad} , $E_{\text{N}}^{\text{diff}}$, is 2.0 eV [15]. The Ehrlich–Schwoebel barrier for N_{ad} to diffuse across the step upwards and downwards are estimated as 10% of $E_{\text{N}}^{\text{diff}}$. Since the Ehrlich–Schwoebel barrier will not influence either the growth morphology or the growth rate in the present work (see Subsection 2.5.) it is of no importance. The value of the energy barrier for reaction (5) is 2.6 eV [21]. The energy barrier for reaction (6), E_{r6} , is 0 eV [14]. The energy barrier for reaction (7), E_{r7} , is 0 eV which is estimated as follows. The

rate of reaction (7) is assumed to be in the same order of magnitude as the rate of the same reaction on the surface of Ir, which is $10^{11} \exp(1.22 \times 10^5 \text{ Jmol}^{-1} / RT)$ [11]. According to Eq. (11) R_{r7} at T_s has the closest value to $10^{11} \exp(1.22 \times 10^5 \text{ Jmol}^{-1} / RT_s)$ when $E_{r7} = 0$ (E_{r7} can not be less than 0 eV). According to Eq. (11), $E_{r7} = 0$ implies that the combination of two AlN_{ad} does not limit the rate of reaction (7) but the knocking between two AlN_{ad} does.

Reaction (8) has 6 growth energy barriers and each one corresponds to one situation with a different number of neighboring AlN dimers. The growth energy barriers are denoted as E_g^i , ($i = 1 \dots 6$) where i is the number of the neighboring AlN dimers. According to Ref. [22], the energy decrease for the formation of one AlN dimer of a AlN single crystal (AlN_c) is 11.52 eV and it was estimated from the data in Ref. [23] that the energy decrease for the formation of a AlN_{ad} molecule is 6.4 eV. This means when the energy of one AlN_{ad} molecule is increased by 6.4 eV it will be in the state of one Al atom and one N atom in the vacuum. Therefore this is the upper limit of the energy barrier for one AlN_{ad} attaching to AlN single crystal. This value is used as the growth barrier with one neighbor ($n = 1$ in Table 2). The growth situation with more neighbors is more similar to the environment of an AlN dimer in the perfect crystal and it is an easier situation for an AlN_{ad} to attach to the crystal. Otherwise this crystalline structure will be less favorite than the amorphous structure or other crystalline structures. Therefore it is assumed that the higher the number of the neighboring AlN dimers, the lower the energy barrier for the attachment of AlN_{ad} , and thus, E_g^i are formulated as $E_g^i = 6.4/i$ eV, ($i = 1 \dots 6$). Since 6.4 eV is the upper limit of the energy barrier of attachments, the rates of AlN_{ad} attaching to the single crystal have been

assigned the possibly lowest values. Though this is not perfectly precise it will allow us to check if AlN attaching could be the rate limiting step compared with other steps. It should be noticed that E_g^i is the energy barrier for the reaction (8) which occurs at a fixed site (the grey site shown in Table 2). It is different from the barrier for diffusing from one site to another.

The size of the grid, dz , for the simulation of the vapor diffusion of Al_g is 0.8 mm. $\Delta t_{diff} = 1 \times 10^{-4}$ s. The system size of the KMC simulation for the comparison between the KMC and the analytical model (see Subsection 3.2.) is 84×50 AlN dimers or $25.7 \text{ nm} \times 15.2 \text{ nm}$. For all the other KMC simulations the system size is 55×50 AlN dimers or $16.7 \text{ nm} \times 15.2 \text{ nm}$.

2.4. Influence of the energy barriers of the growth of AlN_{ad} with different neighboring AlN dimers on the growth morphology

To simplify the expression, the energy barriers of the growth of AlN_{ad} (Reaction (8)) with different number of neighboring AlN dimers are expressed as a growth-barrier vector which is defined as $\{E_g^i\} = (E_g^1, E_g^2, E_g^3, E_g^4, E_g^5, E_g^6)$. The influence of $\{E_g^i\}$ on the growth morphology was studied by the KMC model with only 7 events which are the growth of AlN_{ad} with one to six neighboring AlN_c and the surface diffusion of AlN_{ad} . Three $\{E_g^i\}$ are used in the simulation. The six components of $\{E_g^i\}_1$ are all equal to 2.13 eV. $\{E_g^i\}_2 = (2.53, 2.33, 2.13, 1.93, 1.73, 1.53)$ and $\{E_g^i\}_3 = (3.13, 2.63, 2.13, 1.63, 1.13, 0.63)$. All E_g^3 values are equal to 2.13 eV. The components of $\{E_g^i\}_2$ and $\{E_g^i\}_3$ decrease from E_g^1 to E_g^6 and the decrements are 0.2 eV and 0.5 eV, respectively. In the simulations of this subsection, the AlN_{ad} appears on the surface randomly and each time only one AlN_{ad}

appears. After the AlN_{ad} grows to the single crystal another AlN_{ad} appears. The above mechanism implies that the simulated growth is vapor-adsorption limited.

The initial condition of the KMC simulation is shown in Fig. 4a, which is a stripe of a new layer of the AlN crystal in the middle of a flat (0001) surface. AlN_{ad} will grow to the both sides of the stripe. The periodic boundary conditions are applied in the simulation. The simulated growth morphologies using $\{E_{\text{g}}^i\}_1$, $\{E_{\text{g}}^i\}_2$ and $\{E_{\text{g}}^i\}_3$ after incorporation of 98 AlN_{ad} are shown in Figs. 4b–d. From Fig. 4b it can be seen that when the components of $\{E_{\text{g}}^i\}$ are equal (i.e. the energy barrier does not depend on the number of neighboring AlN dimers), the growth morphology shows a pattern of diffusion-limited aggregation and it is far from the morphology of the step-flow growth. Figure 4c shows that the growth morphology becomes less dendritic and more related to step-flow growth when the components of $\{E_{\text{g}}^i\}$ decrease from E_{g}^1 to E_{g}^6 . If the components of $\{E_{\text{g}}^i\}$ decrease by a larger amount from E_{g}^1 to E_{g}^6 (see Fig. 4d) the simulated morphology shows the pattern of step-flow growth. From the above changes of the growth morphology from the diffusion-limited aggregation to the step-flow pattern we can see that the growth-barrier vector $\{E_{\text{g}}^i\}$ can influence the growth morphology significantly and its values are important for the emergence and the stability of the step-flow growth. The KMC simulations reveal that one of the necessary conditions for step-flow growth is that there has to be a decrease of the energy barrier for the growth with increasing number of neighboring AlN dimers which should exceed some (positive) value. In other words, the growth rate for the growth at places with more neighboring AlN dimers should be reasonably faster than the growth at places with less neighboring AlN dimers.

Previous studies have shown that the growth being fractal or compact depends on the rate ratio between the jump to the step and the jump along the step [24]. In the case of (0001) surface of AlN, due to the Wurtzite structure (similar to hcp) all the jumps are along the directions which are $\pi/3$ away from the normal direction of the step. Therefore it can not be separated which jump is to the step and which one is along the step. In the present model the energy barriers for the jumps to the step and along the step are the same. The transition from the fractal growth to the compact growth is solely due to the different values of the growth-barrier vectors, $\{E_g^i\}$. The components of the growth-barrier vectors actually change the relative growth rates of the six different growth situations. When the growth rate with more neighbors is higher the growth will be more compact. This is the situation where the step tends to keep straight during the growth. In the reverse case the growth will be more fractal. This explains why the transition from the fractal to compact growth can be observed in the present model though the energy barriers for the jumps are all same.

2.5. Simulated morphology of the step-flow growth on the (0001) surface.

The step-flow growth on the (0001) surface of AlN single crystals is simulated by the vapor diffusion coupled KMC model with the parameters of Subsection 2.3. Figure 5a shows the initial condition of the simulation. The number of the steps is 10. The width of each terrace is 1.34 nm. The periodic boundary condition is applied along the direction of the steps. The quasi-periodic boundary condition is used along the direction vertical to the steps. The quasi-periodic boundary condition means when a step (or a particle) runs out of the left side of the system it reappears as a new step (or a new particle) at the right side of the system. The

reverse way is also possible for an particle. Due to the quasi-periodic boundary condition the number of AlN layers can increase without the layer nucleation event.

Figure 5b shows the simulated growth morphology which indicates that the surface has a stable step-flow growth. In fact at 10.0 s 132 new layers have grown. In this figure only the top layers are shown. Figure 5b also shows the details of the surface state. It can be seen that the surface is very clean. There are only two N_{ad} atoms on the surface (the red spheres). This means that the rate of adsorption of Al_g on the surface is much slower than the rate of the surface diffusion and the rates of reactions (5) to (8). This is further validated by the instantaneous rates of the events in the KMC simulation at $t = 6.0$ s (see Table 1). According to Table 1, the rate of adsorption of Al_g is much slower than the other events except the desorption of Al_{ad} and the attachment of AlN_{ad} to the crystal with one neighbor ($n = 1$ in Table 2). The rates of attachments of AlN_{ad} have been assigned the possible lowest values in the KMC simulation but the attachment of AlN_{ad} to the single crystal is still not the rate limiting step according to Fig. 5b. Therefore, the possible rate limiting steps for the growth of AlN crystal are the adsorption of Al_{ad} to the surface and the vapor diffusion of Al_g from the source material to the crystal seed. Since the speeds of the steps are determined by the adsorption of Al_g or the diffusion of Al_g Ehrlich–Schwoebel barrier of N_{ad} has no influence on the growth morphology and growth rate of the single crystal as was pointed out in Subsection 2.3. In addition, due to the high growing temperature (~ 2400 K), the attempt frequency, Γ_0 , could be as high as 10^{13} s^{-1} instead of 10^{12} s^{-1} used in the simulation. Actually a higher Γ_0 will make all the rates of the surface events higher except the rate of the

adsorption of Al_g . This is because the rate of the adsorption of Al_g is independent of the attempt frequency (see Eq. (12)) but the rates of all the other surface events are proportional to the attempt frequency. Therefore a higher Γ_0 will only strengthen the result that the rate of the adsorption of Al_g is much lower than the other surface events.

Figure 6 shows the evolution of Al_g concentration profile from the AlN source (0 mm) to the AlN single crystal (16 mm). The initial condition is that $c_{Al} = 0$ in the vapor phase, i.e. $P_{Al}^s = 0$ and J_{Al}^{out} is at its maximum (see Eq. (16)) and at the same time $P_{Al}^c = 0$ and J_{Al}^{in} is at its minimum (see Eq. (13)). It shows that the concentration profile changes from a upwards-concave curve to a straight line after about 1.5 s. This means the vapor diffusion of Al_g evolves to a steady state very quickly (usually one growth of AlN single crystal takes tens of hours). At the steady state the flux of Al_g going through the vapor phase is constant and it is equal to the fluxes coming out of the source material and going into the adlayer of the single crystal. Because of the coupling with the vapor diffusion model through BC2, as soon as the vapor diffusion reaches the static state the crystal surface simulated by KMC also reaches to the steady state where all the rates and surface concentrations are constant. The short time for the transition to the steady state indicates that the vapor transport is not the rate-limiting step.

The time evolution of the vapor concentration of Al_g in close vicinity to the surface of the AlN source material, c_{Al}^s , is shown in Fig. 7a. It can be seen that c_{Al}^s increases from 0.0 mol m⁻³ and reaches to a constant value after about 1.5 s. The constant value is 0.069 mol m⁻³.

The time evolution of c_{Al}^c which is the vapor concentration of Al_g in close vicinity to the surface of AlN single crystal is shown in Fig. 7b. Because c_{Al}^c is related to the amount of Al_g adsorbed to the surface of the single crystal obtained by the KMC simulation therefore its value fluctuates. However it is shown clearly in Fig. 7b that the average value of c_{Al}^c increases from 0.0 mol m^{-3} and reaches to a constant value after about 1.5 s, which is the same time when c_{Al}^s reaches a constant value. The constant average value of c_{Al}^c is $1.90 \times 10^{-4} \text{ mol m}^{-3}$. The state with the constant c_{Al}^s and c_{Al}^c corresponds to the steady state shown in Fig. 6 (see the straight line there at $t = 1.5 \text{ s}$). According to Eq. (14) $1.90 \times 10^{-4} \text{ mol m}^{-3}$ corresponds to $P_{\text{Al}}^c = 3.7 \text{ Pa}$ which is very low. This means that the steady flow of Al_g is very small. Using the constant c_{Al}^s and c_{Al}^c the growth rate of (0001) surface of the single crystal can be evaluated as follows. The flux of Al_g from the source to the single crystal at the steady state is $J = D_v (c_{\text{Al}}^s - c_{\text{Al}}^c) / L_{\text{sc}} = 2.69 \times 10^{-4} \text{ mol m}^{-2} \text{ s}^{-1}$. The distance between two Al sub-layers in the AlN crystal is 0.25 nm. Thus, the growth rate at the steady state is $13.5 \mu\text{m h}^{-1}$, which agrees with the preliminary experimental result, $15\text{--}30 \mu\text{m h}^{-1}$. This means under the growing conditions applied in this work the rate limiting factor is the tiny flow of Al_g at the steady state. The steady flow of Al_g can be influenced by T_s , T_c , D_v and L_{sc} . The influence of L_{sc} can be considered in the following way. At the steady state

$$P_{\text{Al}}^s - P_{\text{Al}}^c T_s / T_c = s_{\text{sc}} L_{\text{sc}} R T_s \quad (22)$$

where s_{sc} is the slope of the concentration profile between the source and the crystal and the relation

$$P_{\text{Al}}^s = c_{\text{Al}}^s R T_s \quad (23)$$

which is similar to Eq. (14) is used in the derivation of Eq. (22). When L_{sc} is sufficiently small and $T_s \approx T_c$, $P_{Al}^c \approx P_{Al}^s$. Since $J_{Al}^{out} = J_{Al}^{in}$ at the steady state $P_{Al}^c \approx P_{Al}^s \approx P_{Al}^e / 2 \approx 6.1 \times 10^2$ Pa. Because the growth rate is roughly proportional to P_{Al}^c in the present condition which is the step-flow growth and rate of the supply of Al_g is much smaller than the other rates, the value of the growth rate can be estimated as 2.2 mm h^{-1} . This means the growth rate and therefore the steady flow can be increased significantly by decreasing L_{sc} . With the same rationale, increasing D_v has the similar effects on the steady flow as decreasing L_{sc} does.

Therefore the tiny steady flux of Al_g is determined by the processing parameters of the two ends (source material and single crystal) and the vapor phase in middle. For this reason, in order to increase the growth rate of the AlN single crystal the whole PVT growth system that is the source material, the single crystal and the vapor diffusion should be considered comprehensively. However, regarding the side of the single crystal it is clear from the simulation results that the adsorption of Al_g is the rate-limiting step and the PVT growth of AlN single crystals is Al deficient under the growing conditions studied in this work. The statement that the adsorption of Al_g is the rate-limiting step is equivalent to the statement that the rate limiting step is the tiny steady flow of Al_g . This is because at the steady state the flow from the source to the single crystal in the vapor diffusion model is equal to the adsorption flow to the crystal surface from the vapor phase in the KMC model due to the coupling of the two models. Moreover at the steady state the flow from the source to the single crystal in the vapor phase is also equal to the flow going out of the source into the vapor. The flow of Al_g at the steady state is like a state variable which is determined by T_s ,

T_c , D_v and L_{sc} of the system.

3. Study of step-flow growth by the analytical model derived based on the KMC results

Though the vapor diffusion coupled KMC model can provide various detailed information about most of the important processes involved in the PVT growth of AlN, the limitation of the system size makes it incapable or very inefficient to study the growth of a long train of steps. Based on the insights obtained from the KMC simulation, an analytical model which is much easier to be analyzed and solved is proposed and used to study the growth of a train of steps on the (0001) surface.

3.1. The analytical model for the step-flow growth of AlN

According to the KMC simulation the rate of the adsorption of Al_g is much slower than the rates of all the other surface events. This means the velocity of the i -th step in a train of steps (see Fig. 8) is proportional to the amount of Al atoms adsorbed to the terrace in front of it. If the flux of Al_g to the terrace is homogeneous then

$$v_i = k \cdot l_i \quad (24)$$

where l_i is the terrace width of the i -th step; v_i is the velocity of the $(i+1)$ -th step (see Fig. 8); k is a proportional constant. Equation (24) is not a new model of step-flow growth. But it is found in this work that it is appropriate to use this model to study the step-flow growth of AlN. Since the rate of the increase of the terrace width is equal to the velocity difference between the two steps bounding the terrace, the evolution of l_i obeys the following equation:

$$\frac{dl_i}{dt} = v_{i-1} - v_i, (i = 1, 2, 3, \dots) \quad (25)$$

According to Eq. (24) and Eq. (25) l_i can be solved as the following:

$$l_i = e^{-kt} \left[\sum_{m=0}^{i-1} E_m(e^{kt}) \cdot L_{i-m} + \frac{v_0}{k} \left(e^{kt} - \sum_{m=0}^{i-1} E_m(e^{kt}) \right) \right] \quad (26)$$

where L_i is the initial value of $l_i(t)$; $E_m(e^{kt})$ is the m -th term of the Taylor expansion of e^{kt} ; v_0 is the velocity of the 1st step. From Eq. (26) the terrace width of any step at any time can be obtained when the flux of Al_g is homogeneous.

3.2. Validation of the analytical model by comparing the KMC results with the results of the analytical model

In order to check if the analytical model agrees with the vapor diffusion coupled KMC model, the solution of the analytical model is compared with the numerical results from the KMC simulation. The growth of a train of 17 steps was simulated by the KMC model. The periodic boundary condition is applied along the direction of the steps. Along the direction vertical to the steps the quasi-periodic boundary condition is applied to reactions and diffusions but not to the movement of the steps. The displacement evolution curves, $s_i(t)$, of the points on the 3rd, 4th, 5th and 6th step are recorded. The displacement $s_i(t)$ is the distance to the starting position of the i -th step. The relative positions of the i -th step can be found in Fig. 8. The velocity of the 1st step, v_0 , is kept as 0 during the KMC simulation. The initial widths of the steps, L_i , are all equal to 1.34 nm. k of Eq. (24) is $1.8R_{r4}$, where R_{r4} is the rate of reaction (4) and expressed by Eq. (12). The prefactor 1.8 is from the property of (0001)

surface that the ratio of the number of available positions of Al_{ad} to the number of the positions where AlN_{ad} can attach to the crystal is about 1.8. The analytical formula of the displacement evolution of the i -th step is expressed as

$$s_i(t) = \int_0^t v_{i-1}(t') dt' \quad (i = 1, 2, 3, \dots) \quad (27)$$

where $v_i(t)$ is expressed by Eq. (24) and Eq. (26). Figure 9a–d shows the comparison for the 3rd, 4th, 5th and 6th step, respectively. The blue lines are the KMC results and the red lines with dots are the analytical results. Because of the randomness of the KMC method each analytical $s_i(t)$ curve is compared with seven KMC results obtained using different sets of random numbers so that it can be ensured that the comparison is not a result of coincidence. From Fig. 9 it can be seen that the analytical solution agrees well with the KMC simulation. Therefore the basic assumption of the analytical model, Eq. (24), is correct.

3.3. Growth of a train of steps with random initial terrace widths

The growth of a train of steps with random initial terrace widths under the homogeneous and linearly inhomogeneous flux of Al_g is studied numerically in this section. In the following numerical simulations $v_0 = 0$ in Eq. (26), which is generally realistic because no train of steps can move forward forever and it will stop at a place anyway. The place could be the boundary of a crystal surface, an obstacle in the way of the movement etc. In fact the step-flow growth with the assumptions of Eq. (24) and (25) has been studied intensively [25]. However to the best knowledge of the authors there have no studies on the growth of a train of steps whose first step is immobile. Due to this boundary condition, Eq. (26) is different

from the analytical solutions using periodic boundary condition [26]. The focus of this section is to study numerically if the growth instability can be introduced by the fluctuation of the initial terrace widths and the linearly inhomogeneous flux to the surface under the boundary condition that the first step of a train of steps is immobile.

3.3.1. Under the homogeneous flux of Al_g

The random initial terrace widths L_i is expressed as

$$L_i = \bar{L} + \varepsilon_i \quad (28)$$

where \bar{L} is the average terrace width and ε_i is the random fluctuation whose average is 0. The maximum of $|\varepsilon_i|$ is less than \bar{L} because otherwise L_i will be negative, which is unphysical. From Eq. (28) and (26) it can be derived that

$$l_i = e^{-kt} \sum_{m=0}^{i-1} E_m(e^{kt}) \cdot \varepsilon_{i-m} + e^{-kt} \sum_{m=0}^{i-1} E_m(e^{kt}) \cdot \bar{L} \quad (29)$$

Equation (29) indicates that the evolution of l_i is from two parts. One is the second term in Eq. (29) which is exactly the same with the formula for l_i in the case where the initial terrace widths of all the steps are \bar{L} . The other part is the first term in Eq. (29) which is the deviation from the step evolution whose initial terrace widths are all \bar{L} . This deviation is caused by the fluctuation in the initial terrace widths, ε_i . Since there is no analytical solution available for the case where the terrace widths have fluctuation the motion of the steps is solved numerically using the analytical model Eq. (24) and (25).

Figure 10 shows the comparison of the growth of a train of steps A, which has randomness in the initial terrace widths, to the growth of a train of steps B, whose initial terrace widths are all equal. The average and the randomness of the terrace widths of train A are $\bar{L}_A = 1.34$ nm and $\pm 0.5\bar{L}_A$, respectively. The terrace widths of train B are all equal to \bar{L}_A . The flux of Al_g is homogeneous and it is 2.69×10^{-4} mol m⁻² s⁻¹ which is equal to the steady flux of Al_g of the KMC simulation in Subsection 2.5. Figure 10a shows the initial positions of train A (crosses) and that of train B (line with circles). The number of the steps is 30 and $v_0 = 0$ for the both trains. Figure 10b shows the comparison of the step positions of train A and train B at $t = 14848$ s. It can be seen that the randomness in the terrace widths of train A disappears during the growth. In addition it is shown that at $t = 14848$ s the step positions of train A almost overlap those of train B completely. This means l_i with the initial fluctuation ε_i will tend to the evolution path of the case where the initial terrace widths are equal to \bar{L} , which is

$$l_i = e^{-kt} \sum_{m=0}^{i-1} E_m(e^{kt}) \cdot \bar{L} \quad (30)$$

From Eq. (30) it can be seen that when the index i is large, $e^{-kt} \sum_{m=0}^{i-1} E_m(e^{kt}) \approx 1$ and therefore

$$l_i \approx \bar{L} \quad (31)$$

This means for the step terrace far behind the beginning of a train of steps the randomness of the terrace widths will disappear and additionally they will move with the same terrace width which does not change with time and this is just the step-flow growth even though the beginning of the train of steps does not move ($v_0 = 0$). Therefore the solution of the terrace

widths with the periodic boundary condition can be reproduced by Eq. (30) when the step index, i , is large.

Figure 11 shows the numerical calculation of the evolution of the step-positions of train A according to the analytical model. The calculation parameters are the same with the calculation in Fig. 10. Figure 11a is the initial condition of train A and it shows in a different way the same step-positions of train A in Fig. 9a. Figure 11b is the cross section of Fig. 11a. The positions of A and B in Fig. 11b corresponds to the positions of A and B in Fig. 11a, respectively. Figure 11c shows the growth morphology at $t = 14848$ s. Near the end of the train (the part near the line B) the steps have the same terrace width, which is the same as what the analytical analysis indicates (see Eq. (31)). Near the beginning of the train (line A) there is a step-bunching, which is caused by the deceleration of the step-motion close to the beginning of the train which does not move ($v_0 = 0$). Figure 11d is the cross section of Fig. 11c, which shows the step-bunching at the beginning of the train more clearly. Figure 11e shows the growth morphology at $t = 23808$ s. Compared with Fig. 11c it can be seen that the steps near the end of the train moves forwards with the same terrace width as $t = 14848$ s (see Fig. 11c). This is the step-flow growth predicted by the analytical model (see Eq. (31)). Figure 11f is the cross section of Fig. 11e.

3.3.2. Under the inhomogeneous flux of Al_g

The flux of Al_g changes linearly from the beginning to the end of a train of steps. Two cases are studied. One is that the flux at the beginning of the train has the highest value. The other

case is opposite. Since the objective is to study the influence of the linear inhomogeneity of the flux of Al(g) on the stability of the step-flow growth the slope of the linear inhomogeneity of the flux of Al(g) is the parameter that really matters. Due to the fact that a train of steps can grow from the edge of the (0001) crystal plane to the inner of the crystal plane (e.g. nucleate at the edge of the crystal plane) or from the inner to the edge (e.g. spiral growth) it would be both possible for a train of step to grow along the flux gradient or against the flux gradient on the (0001) crystal plane. Therefore both of the cases can occur in the reality. The slope of the change of the flux is estimated in the following way. The radius of the AlN single crystal is assumed to be 2 cm. In the centre the flux is the highest and at the edge the flux is 0. Or vice versa. The highest value of the flux is $2.69 \times 10^{-4} \text{ mol m}^{-2} \text{ s}^{-1}$ which is equal to the steady flux of Al_g of the KMC simulation in the Subsection 2.5. Therefore the slope of the change of the flux is $1.345 \times 10^{-2} \text{ mol m}^{-3} \text{ s}^{-1}$. All the other parameters used are the same with the ones in the numerical calculation in Subsection 3.3.1. According to the result, the randomness of the terrace widths disappears under the linearly inhomogeneous flux of Al_g for both of the cases that are studied.

The disappearance of the randomness of the terrace widths under the homogeneous and the linearly inhomogeneous flux of Al_g reveals that the conditions under which our analytical model is valid are the suitable conditions for the stable step-flow growth. Since crystals growing in the stable step-flow mode typically have better structural quality, these conditions are also the suitable conditions for the PVT growth of AlN. The condition under which the analytical model is valid is that the rates of the surface events including both the surface

reactions and the surface diffusion should be much faster than the rate of the supply of Al atoms from the vapor. Therefore there are two directions to fulfill this condition in the process of AlN growth. One is to decrease the rate of the supply of Al_g . The other is to increase the rates of the surface events. Preliminary growth experiments indicate that increasing the N_2 pressure will enlarge the (0001) surface facet and improve the quality of the crystal. This agrees with our results because increasing the N_2 pressure will decrease the D_v and therefore decrease the flow of Al_g at the static state and then the step-flow growth is more stable.

4. Summary and conclusions

A KMC model for the growth of AlN by the PVT method is developed. This KMC model is coupled with a vapor diffusion model for Al_g . By this coupling, the events on the crystal surface and the vapor diffusion of Al_g can interact with each other and the multi-scale simulation of the growth of AlN can be carried out. The growth of the Al-polar (0001) plane of AlN by the PVT method is studied by this diffusion coupled KMC model. The events that are accounted for in the model include the vapor diffusion of Al_g , surface diffusion of Al_g , N_{ad} and AlN_{ad} and reactions (4) to (8). Based on the simulation results of the vapor diffusion coupled KMC model, an analytical model for the step-flow growth is proposed. The influence of the randomness of the terrace widths on the step-flow growth was studied by the analytical model. According to results obtained by the diffusion coupled KMC model and the analytical model of the step-flow growth the following conclusions are drawn:

1. By the results of the diffusion coupled KMC model, it is found that under the growing

conditions of this work the rate limiting step for the PVT growth of AlN is the supply of Al atoms due to the tiny flow of Al_g at the steady state.

2. The energy barriers for the growth of AlN_{ad} with different neighboring AlN dimers of crystal can influence the growth morphology significantly. To have step-flow growth, the energy barrier for the growth of AlN_{ad} to the crystal with more neighboring AlN dimers of crystal should be significantly lower enough than the growth barrier with less neighboring AlN dimers.

3. For the step-flow growth, the step-bunching caused by the randomness of the terrace widths can be avoided for both homogeneous and linearly inhomogeneous flux of Al_g if the rates of the surface events are much faster than the rate of the supply of Al atoms from the vapor.

Acknowledgement

Financial support from the Deutsche Forschungsgemeinschaft (DFG-No. EM 68/27-1) is greatly acknowledged.

References

- 1 T. D. Cutler and J. J. Zimmerman, *Anim. Health Res. Rev.*, 2011, **12**, 15 - 23.
- 2 M. Kneissl, T. Kolbe¹, C. Chua, V. Kueller, N. Lobo¹, J. Stellmach¹, A. Knauer, H. Rodriguez, S. Einfeldt, Z. Yang, N. M. Johnson and M. Weyers, *Semicond. Sci. Technol.*, 2011, **26**, 014036 - 014036.

- 3 E. R. Meinders, R. Rastogi, M. Van der Veer, P. Peeters, H. El Majdoubi, H. Bulle, A. Millet and D. Bruls, *Jpn. J. Appl. Phys.*, 2007, **46**, 3987 - 3992.
- 4 K. Ban, J. Yamamoto, K. Takeda, K. Ide, M. Iwaya, T. Takeuchi, S. Kamiyama, I. Akasaki and H. Amano, *Appl. Phys. Express*, 2011, **4**, 052101.
- 5 H. Hirayama, S. Fujikawa, N. Noguchi, J. Norimatsu, T. Takano, K. Tsubaki and N. Kamata, *Physica Status Solidi A Appl. Res.*, 2009, **206**, 1176 - 1182.
- 6 M. Kneissl, Z. Yang, M. Teepe, C. Knollenberg, O. Schmidt, P. Kiesel, N. M. Johnson, S. Schujman and L. J. Schowalter, *J. Appl. Phys.*, 2007, **101**, 123103.
- 7 T. Wunderer, C. L. Chua, Z. Yang, J. E. Northrup, N. M. Johnson, G. A. Garrett, H. Shen and M. Wraback, *Appl. Phys. Express*, 2011, **4**, 092101.
- 8 A. B. Bortz, M. H. Kalos and J. L. Lebowitz, *J. Comp. Phys.*, 1975, **17**, 10 - 18.
- 9 D. T. Gillespie, *J. Comp. Phys.*, 1976, **22**, 403 - 434.
- 10 K. A. Fichthorn and W. H. Weinberg, *J. Chem. Phys.*, 1991, **95**, 1090 - 1096.
- 11 C. J. Weststrate, J. W. Bakker, E. D. L. Rienks, S. Lizzit, L. Petaccia, A. Baraldi, C. P. Vinod and B. E. Nieuwenhuys, *J. Chem. Phys.*, 2005, **122**, 184705.
- 12 B. M. Epelbaum, M. Bickermann, S. Nagata, P. Heimann, O. Filip and A. Winnacker, *J. Cryst. Growth*, 20017, **305**, 317 - 325.
- 13 P. M. Dryburgh, *J. Cryst. Growth*, 1992, **125**, 65 - 68.
- 14 Z. Romanowski, S. Krukowski, I. Grzegory and S. Porowski, *J. Chem. Phys.*, 2001, **114**, 6353 - 6363.
- 15 V. Jindal and F. Shahedipour-Sandvik, *J. Appl. Phys.*, 2009, **105**, 084902-1 - 084902-6.
- 16 D. W. Greenwell, B. L. Markham and F. Rosenberger, *J. Cryst. Growth*, 1981, **51**, 413 -

425.

- 17 M. Hoch and D. Ramakrishnan, *J. Electrochem. Soc.*, 1971, **118**, 1204 - 1211.
- 18 M. W. Chase Jr., *NIST-JANAF Thermochemical Tables*, Woodbury, New York, 1998.
- 19 H. Schulz and K. H. Thiemann, *Solid State Commun.*, 1977, **23**, 815 - 819.
- 20 C. Ratsch and M. Scheffler, *Phys. Rev. B*, 1998, **58**, 13163 - 13166.
- 21 B. Cao, A. K. Starace, O. H. Judd and M. F. Jarrold, *J. Am. Chem. Soc.*, 2009, **131**, 2446 - 2447.
- 22 D. Powell, M. A. Migliorato and A. G. Cullis, *Phys. Rev. B*, 2007, **75**, 115202-1 - 115202-9.
- 23 Aurora Costales, M. A. Blanco, E. Francisco, A. Martin Pendas and Ravindra Pandey, *J. Phys. Chem. B*, 2006, **110**, 4092 - 4098.
- 24 S. Krukowski and J. C. Tedenac, *J. Cryst. Growth*, 1996, **160**, 167 - 176.
- 25 C. Misbah, O. Pierre-Louis and Y. Saito, *Rev. Mod. Phys.*, 2010, **82**, 981-1040.
- 26 R. L. Schwoebel and E. J. Shipsey, *J. Appl. Phys.*, 1966, **37**, 3682-3686.

List of table and figure captions

Table 1: The events included in the KMC model and their instantaneous rates in the simulation at $t = 6.0$ s.

Table 2: Different situations where reaction [8] can occur. Grey points (always in the centre) represent AlN_{ad} particles. Black points represent the AlN_{c} molecules. White points represent the empty sites.

Figure 1: (Color online) Schematic illustration of the PVT growth of an AlN single crystal. T_{c} is the temperature of the AlN single crystal seed. T_{s} is the temperature of the AlN source material.

Figure 2: Illustration of the area of one available position for the Al_{ad} , $S_{\text{Al}}^{\text{ad}}$. The area of the regular triangle ABC is $S_{\text{Al}}^{\text{ad}}$. The circles of the solid line is one layer higher than the circles of the dotted line.

Figure 3: (Color online) The estimated potential energy surface (PES) of AlN_{ad} , which is the overlapping of PESs of Al_{ad} and N_{ad} on N-terminated (0001) surface of AlN [15].

Figure 4: (Color online) The influence of the growth-barrier vector $\{E_{\text{g}}^i\}$ on the growth morphology. (a) Initial condition. (b)–(d) Growth morphologies obtained with $\{E_{\text{g}}^i\}_1 = (2.13, 2.13, 2.13, 2.13, 2.13, 2.13)$, $\{E_{\text{g}}^i\}_2 = (2.53, 2.33, 2.13, 1.93, 1.73, 1.53)$ and $\{E_{\text{g}}^i\}_3 = (3.13, 2.63, 2.13, 1.63, 1.13, 0.63)$, respectively. (b)–(d) were output when the number of AlN_{ad} growing to the crystal reaches 98.

Figure 5: (Color online) KMC simulation of the growth morphology of (0001) surface of the AlN single crystal. (a) Initial condition (b) Growth morphology at $t = 10.0$ s The N_{ad} atoms are shown in red.

Figure 6: Al vapor concentration profile evolution obtained by the vapor transportation model coupled with the KMC model. 0 mm is the position of the source material. 16 mm is the position of the single crystal seed. After about 1.5 s, the diffusion of Al_{g} evolves to a steady state.

Figure 7: (a) Time evolution of c_{Al}^{s} which is the vapor concentration of Al_{g} next to the surface of the AlN source material. (b) Time evolution of c_{Al}^{c} which is the vapor concentration of Al_{g} next to the surface of the AlN single crystal. Both of the concentrations first increase from 0.0 mol m^{-3} and then reach to a constant value after about 1.5 s. The state with the constant c_{Al}^{s} and c_{Al}^{c} corresponds to the steady state shown in Fig. 6 (see the straight line there at $t = 1.5$ s).

Figure 8: Schematic illustration of the step-flow growth. l_i is the terrace width of the i -th step. v_i is the velocity of the $(i+1)$ -th step. s_i is the displacement of the i -th step from its starting position.

Figure 9: (Color online) Comparison between the analytical model (red lines with dots) and the KMC simulation (blue lines). (a) to (d) are the comparison of the displacement evolution

curves of the 3rd step to the 6th step, respectively. Please refer to Fig. 8 for the relative step-positions in the step-train. Each analytical solution is compared with seven KMC results. The analytical solution and the KMC results are in good agreement.

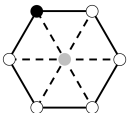
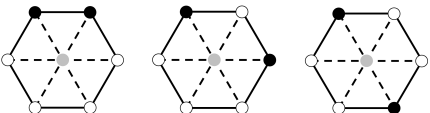
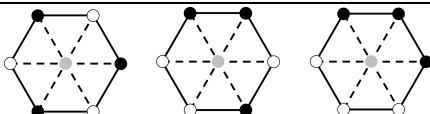
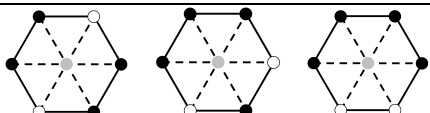
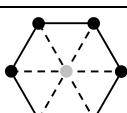
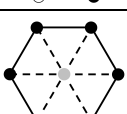
Figure 10: (Color online) Comparison of the growth of a train of steps A, which has randomness in the initial terrace widths (crosses), to the growth of a train of steps B, whose initial terrace widths are all equal (line with circles). The flux of Al_g is homogeneous. (a) comparison at $t = 0$ s. (b) comparison at $t = 14848$ s. The randomness in the terrace widths of train A disappears. The step positions of train A tends to be the same with that of train B.

Figure 11: (Color online) The growth of the train of steps A (the same one in Fig. 10) with homogeneous flux of Al_g . (a) Initial step positions of train A. $t = 0$ s. (b) The cross section of (a). The positions of A and B corresponds to the positions of A and B in (a), respectively. (c) Step positions at $t = 14848$ s. Near the end of the train (the part near line B) the steps have the same terrace width. Near the beginning of the train (line A) there is a step-bunching, which is caused by $v_0 = 0$. (d) The cross section of (c). (e) Step positions at $t = 23808$ s. The steps near the end of the train moves with the same terrace width as in (c), which indicates this is step-flow growth. (f) The cross section of (e).

Table 1: The events included in the KMC model and their instantaneous rates in the simulation at $t = 6.0$ s.

Events in the KMC model	Rate of the events (s^{-1})
Diffusion of Al_{ad}	1.90×10^7
Diffusion of N_{ad} on the same terrace	5.10×10^7
Diffusion of N_{ad} across the step downwards	1.90×10^7
Diffusion of N_{ad} across the step upwards	1.90×10^7
Diffusion of AlN_{ad}	1.51×10^8
Reaction (1): Adsorption of Al_g $Al_g \Rightarrow Al_{ad}$	1.08×10^1
Reaction (1): Desorption of Al_{ad} $Al_g \Leftarrow Al_{ad}$	1.33×10^{-1}
Reaction (2): $Al_{ad} + N_2 = AlN_{ad} + N_{ad}$	2.63×10^6
Reaction (3): $Al_{ad} + N_{ad} = AlN_{ad}$	7.00×10^7
Reaction (4): $N_{ad} + N_{ad} = N_2 (g)$	1.02×10^8
Reaction (5): $AlN_{ad} \Rightarrow AlN_c$ with 1 neighbor ($m = 1$)	1.84×10^{-2}
Reaction (5): $AlN_{ad} \Rightarrow AlN_c$ with 2 neighbors ($m = 2$)	1.36×10^5
Reaction (5): $AlN_{ad} \Rightarrow AlN_c$ with 3 neighbors ($m = 3$)	2.64×10^7
Reaction (5): $AlN_{ad} \Rightarrow AlN_c$ with 4 neighbors ($m = 4$)	3.68×10^8
Reaction (5): $AlN_{ad} \Rightarrow AlN_c$ with 5 neighbors ($m = 5$)	1.79×10^9
Reaction (5): $AlN_{ad} \Rightarrow AlN_c$ with 6 neighbors ($m = 6$)	5.14×10^9

Table 2: Different situations where reaction [8] can occur. Grey points (always in the centre) represent AlN_{ad} particles. Black points represent the AlN_c molecules. White points represent the empty sites.

Number of neighbors	Configurations
$n = 1$	
$n = 2$	
$n = 3$	
$n = 4$	
$n = 5$	
$n = 6$	

The step-flow growth of the PVT-grown AlN single crystal is studied by a multi-scale model developed in this work which takes into accounts both surface reactions and material transport in vapor phase.

